Journal of Ceramic Processing Research. Vol. 27, No. 1, pp. 67~70 (2026)
(Received 20 August 2025, Received in revised form 24 January 2026, Accepted 26 January 2026)
https://doi.org/10.36410/jcpr.2026.27.1.67

J O U R N A L O F
Ceramic Processing Research

Enhanced temperature stability of small-permittivity $Li_3Mg_2SbO_5F_2$-basic microwave dielectric ceramics through $Ba_3(VO_4)_2$ addition

Cuijin Pei[a], Fanfan Pan[a], Qianjing Jia[a], Li Quan[a], Miao Chen[a], Weihong Liu[b], Guoguang Yao[a,*], Wei Zhang[a,*] and Yansheng Wang[c]

[a]*School of Science, Xi'an University of Posts and Telecommunications, Xi'an 710121, China*
[b]*School of Electronic Energineering, Xi'an University of Posts and Telecommunications, Xi'an 710121, China*
[c]*Xi'an Chaofan Optoelectronic Equipment Co., LTD, Xi'an 710121, China*

Microwave ceramics with close-zero temperature coefficient of resonance frequency (τ_f~0 ppm/◦C) high quality factor (Q×f>50,000 GHz), small permittivity (ε_r<15), and low sintering temperature (Ts<950 ºC) are gaining great attention in the field of fundamental research and 5G communication. Until now, ceramics owing aforementioned key metrics at the same time is quite rare. In this paper, the (1-*x*)$Li_3Mg_2SbO_5F_2$–*x*$Ba_3(VO_4)_2$ (*x*=0.2–0.4) counterparts had been fabricated through high temperature solid state reaction at 750–850 ºC. X-ray diffraction and SEM-EDS analyses showed all the specimens are composed of two dissimilar phases: $Ba_3(VO_4)_2$ and $Li_3Mg_2SbO_5F_2$. The ε_r, τ_f and Q×f of $Li_3Mg_2SbO_5F_2$-host counterpart upgrade with the increase of $Ba_3(VO_4)_2$ content, and a near-zero τ_f is obtained for the specimen with *x*=0.3. With increment of sintering temperature, the volume density, Q×f together with ε_r for 0.7$Li_3Mg_2SbO_5F_2$–0.3$Ba_3(VO_4)_2$ ceramics rose first and reduced thereafter, yet its τ_f remained stable. An expected ε_r of 11.4, τ_f of 4.8 ppm/ºC and Q×f of 50,600 GHz were achieved at *x* = 0.3 constituent sintered at 825 ºC.

Keywords: Composite ceramics, $Li_3Mg_2SbO_5F_2$ oxyfluorides, $Ba_3(VO_4)_2$, Temperature stability.

Introduction

Recently, Li-containing oxyfluoride ceramics are drawing tremendous attentions owing to their fascinating low sintering temperature as well as eminent microwave dielectric properties (MDPs) [1–5]. Within the Sb_2O_5-LiF–Li_2O–MgO system, a novel oxyfluoride namely, $Li_3Mg_2SbO_5F_2$, was reported. We found that the 825 ºC-sintered $Li_3Mg_2SbO_5F_2$ oxyfluoride ceramics possess eminent MDPs at 9.2 GHz (ε_r =8.1, Q×f = 68, 500 GHz, τ_f = -54 ppm/◦C) [6]. Yet, its high negative τ_f value (-54 ppm/ºC) of $Li_3Mg_2SbO_5F_2$ oxyfluoride ceramics impedes its practical applications to a great extent [7]. There are two primary approaches to modulate the MDPs, especially for τ_f: 1) selecting two compounds with converse τ_f to construct diphase ceramics and 2) by ion replacement to construct a solid solution [8–10]. The solid solution $Sr_{1+2x}La_{2-2x}Al_{2-2x}Ti_{2x}O_7$ (*x* = 0.55, τ_f ≈3.3 ppm/ºC) and (1-*x*)$Mg_6Ti_5O_{16}$-*x*$Ca_{0.8}Sr_{0.2}TiO_3$ diphase ceramics (*x* = 0.22, τ_f ~ -1.28 ppm/ºC) are the most suitable samples among the situations aforementioned [11, 12].

With this regard, the $Ba_3(VO_4)_2$ with positive τ_f (40.0 ppm/ºC) was introduced to tune the MDPs of $Li_3Mg_2SbO_5F_2$-host ceramics [13, 14]. Thus, the (1-*x*)$Li_3Mg_2SbO_5F_2$–*x*$Ba_3(VO_4)_2$ (*x*=0.2-0.4) diphase ceramics were designed and fabricated based on a solid state reaction at 750–850 ºC. The impact of $Ba_3(VO_4)_2$ addition on the phase constituents, sintering behavior, microstructures together with MDPs of the 0.3$Li_3Mg_2SbO_5F_2$–0.7$Ba_3(VO_4)_2$ sintered specimens was thoroughly investigated.

Experimental

Through a solid-state process the (1-*x*)$Li_3Mg_2SbO_5F_2$–*x*$Ba_3(VO_4)_2$ (*x*=0.2-0.4) (abbreviated as LMSOF-BV) specimens were fabricated. Based on stoichiometric $Li_3Mg_2SbO_5F_2$ and $Ba_3(VO_4)_2$, the initial materials of MgO, Li_2CO_3, MgF_2, V_2O_5, $BaCO_3$ (all purity>98.0 %) were separately weighed, then were individually mixed via planetary milling for 9 h with anhydrous alcohol as medium. The dried $Li_3Mg_2SbO_5F_2$ and $Ba_3(VO_4)_2$ slurries were individually presintered under 750 ºC/4 h and 650 ºC/20 h. Subsequently, the LMSOF-BV mixture powders were re-milled for 9 h. By adding 6 wt% PVA binder, the above mixture powders were granulated, and compacted into green discs with diameter of 10 mm and thickness around 4.5 mm. Finally, these discs were fired under 750 ºC–850 ºC for 5 h in air atmosphere.

The phase identification, structural investigation along with fracture surface morphology of the LMSOF-BV samples were examined via X-ray diffraction (XRD,

*Corresponding author:
Tel : +86 29 88166089
E-mail: yaoguoguang@xupt.edu.cn, zhangweio@xiyou.edu.cn

Japan) and scanning electron microscopy (SEM, Czech). The volume densities of fired specimens were trialed employing Archimedes' drainage approach. With the help of resonant cavity method, the ε_r and Qxf values under microwave region about 10–11 GHz of the LMSOF-BV ceramics were measured employing a vector network analyzer (Ceyer 3674D). The τ_f values were evaluated based on following expressions (1) [15].

$$\tau_f = \frac{f_{85} - f_{25}}{f_{25} \times (85 - 25)} \quad (1)$$

Results and Discussion

Table 1 summarizes the MDPs of 825 °C-sintered LMSOF-BV ceramics systems. As *x* rose from 0.2 to 0.4, the ε_r, τ_f and Qxf values gradually increased. An excellent overall MDPs could be obtained for the composition of *x*=0.3. Thereby, the following investigation was focused on the *x*=0.3 composition ceramics.

Fig. 1 gives the XRD plots of 0.7LMSOF-0.3BV ceramics sintered at 750–850 °C. All sintered bodies exhibited a similar phase assemble. All diffraction peaks match well with trigonal structural phase of $Ba_3(VO_4)_2$ (PDF #71-2060) and $Li_3Mg_2SbO_5F_2$ [6, 16]. The achieved outcomes indicated the diphase ceramics of

Table 1. Microwave dielectric properties for (1-x)LMSOF-xBV ceramics fired at 825 °C.

Composition	ε_r	Qxf (GHz)	τ_f (ppm/°C)
x=0.2	10.6	31,700	–10.6
x=0.3	11.4	50,600	4.8
x=0.4	11.9	56,900	18.6

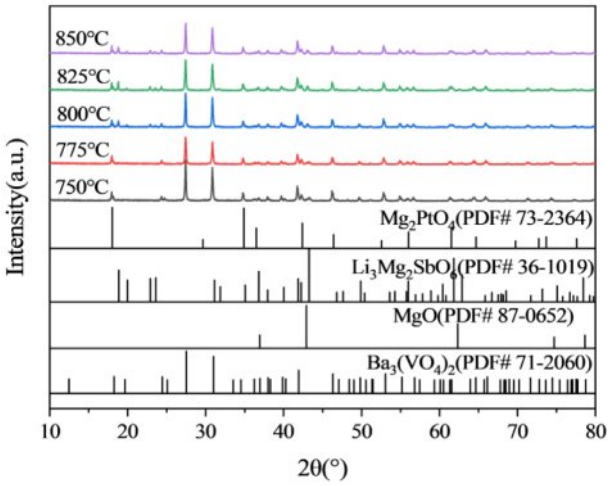

Fig. 1. The XRD plots of 0.7LMSOF-0.3BV sintered at 750–850 °C.

$Li_4Mg_2SbO_6F/Ba_3(VO_4)_2$ was formed without noticeable secondary phases, which could attribute to their diverse crystal structure [17].

Fig. 2(a)–(f) display the fracture surface graphs and corresponding EDS spectra of 0.7LMSOF-0.3BV ceramics sintered at unlike temperatures. The 775 °C-sintered samples exhibited large number of intergranular pores, which tallied well with its poor density, as illustrated in Fig. 2(a) and Fig. 3. As the firing temperature rose, the intergranular pores declined and average grain size along with the homogeneity of grain size distribution grew. A dense microstructure accompanied by a relative uniform grain size distribution were gained for 825 °C-heated ceramics. Further increment the temperature to 850 °C, an unevenly grown grain emerged, as seen in Fig. 2(d), which would deteriorate the dielectric

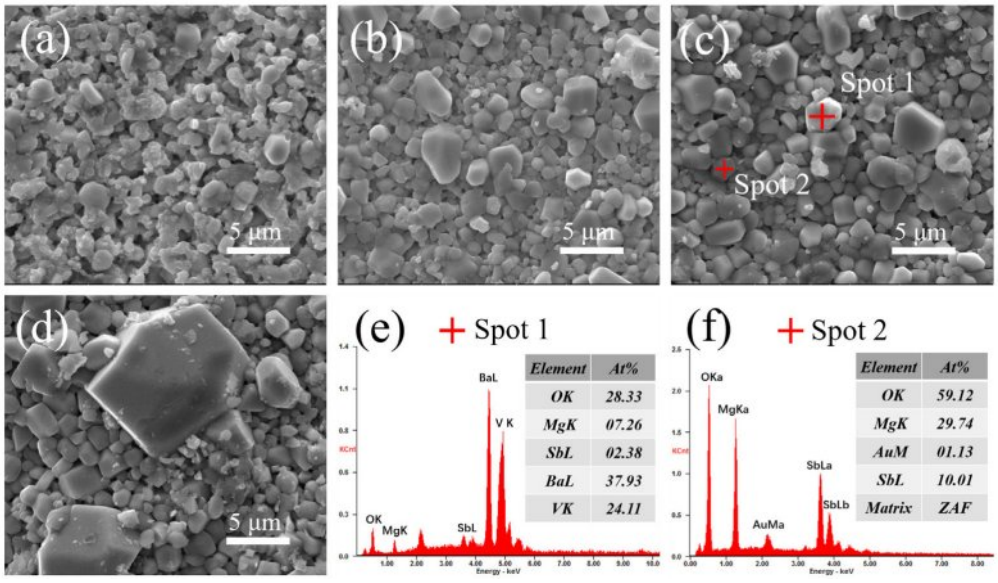

Fig. 2. The fracture surface graphs and corresponding EDS spectra of various temperature sintered 0.7LMSOF-0.3BV ceramics: (a) 775 °C, (b) 800 °C, (c) 825 °C, (d) 850 °C, (e) EDS spectra of spot 1, (f) EDS spectra of spot 2.

properties [18]. Moreover, all samples comprised two distinct-colored grains (white and black) marked in in Fig. 2(c). EDS analysis was carried out to identify the elemental composition of distinct-colored grains, and the resultant outcomes are presented in Fig. 2(e) and (f). Where the Ba and V element are enriched in white colored grains (spot 1), while Mg and Sb are enriched in black colored grains (spot 2), suggesting that white and black colored grains respectively corresponded to $Ba_3(VO_4)_2$ and $Li_3Mg_2SbO_5F_2$ phase, which tallied well with the aforementioned XRD results.

The density and shrinking ratio of 0.7LMSOF-0.3BV under different temperature sintering are displayed in Fig. 3 The density and shrinking ratio showed a similar tendency, initially rising and then reducing as sintering temperature rose. The increase in density and shrinking ratio could ascribe to that the gases from the pores within the ceramics flee with an increasement in firing temperature, the ceramics shrinks and thus brings about its density increment [19]. The decrease in density was due to the unevenly grown grain, as seen the SEM image in Fig. 2(d).

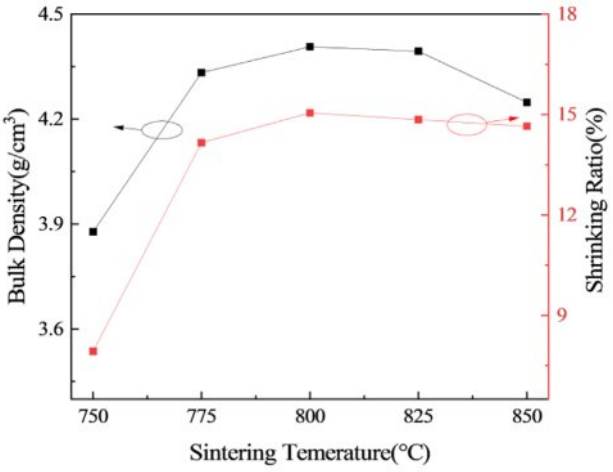

Fig. 3. The density and shrinking ratio of 0.7LMSOF-0.3BV under different temperature sintering.

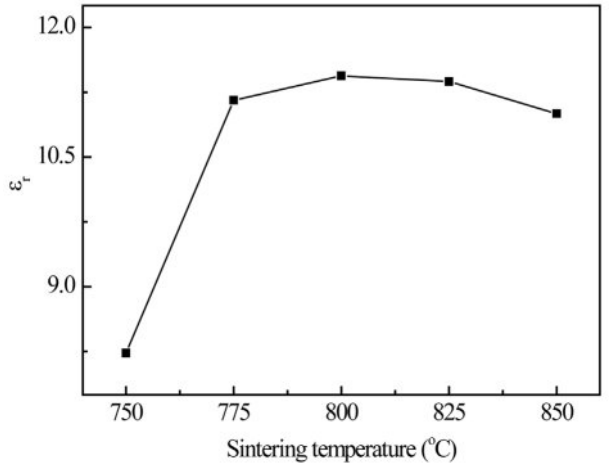

Fig. 4. The ε_r of the 0.7LMSOF-0.3BV samples under different sintering temperature.

The dependence of ε_r over sintering temperature of the 0.7LMSOF-0.3LSO samples is exhibits in Fig. 4. The variation of ε_r with sintering temperature roughly shows an analogous inclination to that of densities (Fig. 2), since ε_r in microwave frequency is chiefly influenced by porosity for a fixed composition [20]. The ε_r of present ceramics displayed a stepwise increment with the wake of firing temperature, achieve a maximum value of 11.4 under 800 °C, and slightly declined with further increasing temperature. An abatement in porosity induces an increment in ε_r of present ceramics, because the ε_r of pores is near to 1. Additionally, an increase in average grain size also leads to an increase in ε_r due to the reduction in grain boundaries [21].

Figure 5 exhibits the change of Q×f and τ_f for the 0.7LMSOF-0.3BV composites over firing temperature. The change tendency of Q×f values over firing temperature is slightly different from the density and ε_r, because the influencing factors of Q×f are more complex, including intrinsic and non-intrinsic losses [22]. The present ceramics displayed a stepwise increment in Q×f values with the wake of firing temperature, achieve a peak value of 50,600 GHz at 825 °C, and slightly declined in the end with further increasing temperature. Generally, the intrinsic loss is very low, whereas the extrinsic loss largely contributes to the total dielectric loss at microwave frequencies and it is very important to overcome these losses. The increment in Q×f values goes hand in hand with the increment in density along with the reduction of grain boundaries (Fig. 2), whereas the reduced Q×f values at 850 °C is due to the appeared unevenly grown grain in Fig. 2(d) [23]. With regard to τ_f (Fig. 5), the τ_f values is relatively independence to sintering temperature, which remain relatively stable at around 4.8 ppm/°C. The τ_f value depends on the amount of agent, the constitution as well as the existence of a second phase [24-26]. In current ceramics, the relatively

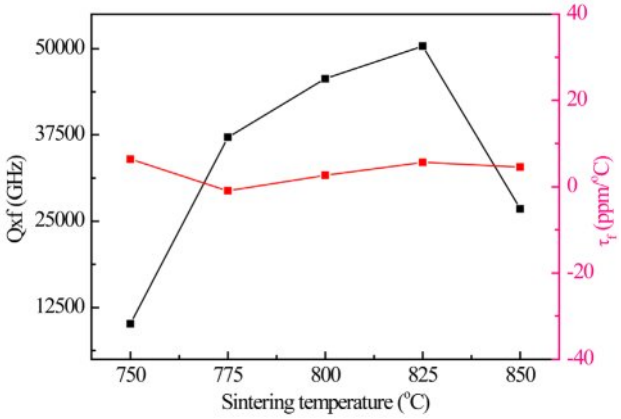

Fig. 5. The Q×f and τ_f of the 0.7LMSOF-0.3BV composites under different sintering temperature.

stable τ_f can attribute to its unchanged phase assemble with sintering temperature (seen in Fig. 1).

Conclusions

In this work, (1-*x*)$Li_3Mg_2SbO_6F$–*x*$Ba_3(VO_4)_2$ (*x*=0.2–0.4) diphase ceramics were fabricated through high temperature solid state reaction route at 750–850 ℃. The two phases $Li_3Mg_2SbO_5F_2$ and $Ba_3(VO_4)_2$ coexist harmoniously as confirmed by XRD and SEM-EDS analyses. The introduction of $Ba_3(VO_4)_2$ can not only significantly ameliorate the τ_f, but also improve the Q×f and ε_r of $Li_4Mg_2SbO_6F$-host counterpart. For the *x*=0.3 composition, its ε_r and Q×f is chiefly influenced by density and overinflated grain coarsening, whereas its τ_f is chiefly influenced phase assemble. 825 ℃-sintered $0.7Li_3Mg_2SbO_6F$–$0.3Ba_3(VO_4)_2$ diphase ceramics exhibited excellent overall MDPs (ε_r of 11.4, Q×f of 50,600 GHz and τ_f of 4.8 ppm/◦C), thereupon showcasing the tremendous potential for LTCC applications.

Acknowledgements

This work was funded by grants from National Natural Science Foundation of China (No. 52272122, No. 52002317), Service Local Special Plan Project of Shaanxi Province Education Department (No. 24JC082), Xi'an Sciences Plan Project (No. 25GXKJRC00053).

References

1. C. Huang, J. Zhang, J. Gu, Q. Li, and J. Yang, J. Eur. Ceram. Soc. 45 (2025) 117699.
2. Z.X. Fang, H.F. Peng, D.Y. Liang, Y.X. Li, B. Tang, and M. Zhang, Ceram. Int. 50 (2024) 43513-43521.
3. Z.G. Hou, Y.X. Li, F. Wang, D.Y. Liang, B. Tang, and W. Liu, Ceram. Int. 50 (2024) 46542-46547.
4. R. Li, X.B. Zhou, S.M. Zhai, S.F. Hou, P. Shi, and P. Liu, Ceram. Int. 51[7] (2025) 8824-8831.
5. C.J. Pei, H.K. Liu, M. Chen, F. Shang, W.H. Liu, and G.G. Yao, Ceram. Int. 50 (2024) 51718-51723.
6. P.S.Wu, C.J. Pei, M. Chen, X. Gao, W.H. Liu, G.G. Yao, and J. Liu, J. Ceram. Process. Res. 24[6] (2023) 977-982.
7. M. Shehbaz, C. Du, R.T. Li, W. Wang, A.R.H. Alzakree, X.G. Yao, H.Y. Peng, H.X. Lin, Z.Q. Shi, D.M. Xu, S. Xia, Y.Q. Pang, and D. Zhou, ACS. Appl. Mater. Interfaces. 14 (2024) 6120-6130.
8. F.L. Liu, J. Li, Y.H. Sun, Y. Tang, and L. Fang, Ceram. Int. 51 (2025) 7370-7376.
9. G.G. Yao, J.J. Tan, J.X. Yan, M.Q. Liu, C.J. Pei, and Y.M. Jia, Ceram. Int. 47 (2021) 27406-27410.
10. A.R.H. Alzakree, C.H. Wan, and M. Shehbaz, J. Am. Ceram. Soc. 108 (2025) e20504.
11. C.D. Hou, Z. Wang, J.T. Kang, Y. Xue, Z. Liu, Z.Y. Ning, J.K. Xie, and X. Li, J. Eur. Ceram. Soc. 45[13] (2025) 117493.
12. S. Ma, X.H. Zhang, J. Zhang, X.H. Zhang, Y. Liu, C.L. Yu, and Z.X. Yue, ACS. Appl. Mater. Interfaces. 17 (2025) 6488-6501.
13. C.H. Su, F.C. Lin, T.M. Chu, and C.L. Huang, J. Alloys Compd. 686 (2016) 608-615.
14. R. Umemura, H. Ogawa, A.Yokoi, H. Ohsato, and A. Kan, J. Alloys Compd. 424 (2006) 388-393.
15. H. Liu, L. Cao, and K.X. Song, J. Eur. Ceram. Soc. 45[2] (2025) 116957.
16. C.S. Lim, J. Ceram. Process. Res. 13[4] (2012) 432-436.
17. G.G. Yao, Z.Y. Ren, and P. Liu, J. Electroceram. 40 (2018) 144-149.
18. C.Z. Yin, H.C. Xiang, C.C. Li, H. Porwal, and L. Fang, J. Am. Ceram. Soc. 101[10] (2018) 4608-4614.
19. Y.J. Liu, G.Q. He, and H.F. Zhou, Ceram. Int. 50 (2024) 36440-36447.
20. X.H. Zhang, X.H. Zhang, S. Ma, X.Y. Qi, and Z.X. Yue, Ceram. Int. 50[9] (2024) 15831-15839.
21. Y.C. Lee, H.J. Shih, T.Y. Wang, and C. Pithan, J. Eur. Ceram. Soc., 44[10] (2024) 5659-5667.
22. P.F. Lv, Y.P. Pu, X.Q. Zhang, X. Lu, C.H. Wu, L. Zhang, B. Wang, Y.T. Ning, J.B. Zhang, and Y.L. Yang, Ceram. Int. 51 (2025) 13514-13521
23. S.L. Zhang, P.P. Ma, X.Q. Liu, and X.M. Chen, J. Am. Ceram. Soc. 98[10] (2015) 3185-3191.
24. X.S. Lv, L.X. Li, H. Sun, S. Li, and S. Zhang, Ceram. Int. 41 (2015) 15287-15291.
25. H.J. Wang and J.J. Bian, J. Eur. Ceram. Soc. 44[4] (2024) 2144-2149.
26. R.Z. Zuo, J. Zhang, J. Song, and Y.D. Xu, J. Am. Ceram. Soc. 101[2] (2018) 569-576.